Low-Cost Embedded System for PMSG Micro-Generator Synchronization Based on the Kuramoto Model

Adan Rincón-Silva[1], R. R. Rivera-Durón[1], R. Sevilla-Escoboza[1], and Onofre Orozco-López[1†]

***Abstract*— The efficient integration of wind micro-generation systems requires complex synchronization schemes, which can be costly due to power electronics and high-level processing units. Furthermore, classical hierarchical control topologies exhibit vulnerabilities, as the disconnection or failure of a leader unit can destabilize the grid. This paper presents a low-cost embedded architecture for the sensorless frequency synchronization of Permanent Magnet Synchronous Generators (PMSG) using an approach based on the Kuramoto oscillator model. The implemented system utilizes an ESP32-S3 microcontroller to execute an SRF-dqPLL algorithm, estimating the frequency and instantaneous phase of each generator. Rather than relying on a hierarchical synchronization strategy, the proposed architecture models each generator as a nonlinear oscillator whose frequency evolves cooperatively through consensus-based coupling dynamics until stable synchronization is achieved.**

I. INTRODUCTION

The paradigm shift toward micro-generation demands modular, robust, and flexible interconnection strategies [1]. This work presents a low-cost embedded system for the sensorless synchronization of low-voltage Permanent Magnet Synchronous Generators (PMSGs) operating in parallel without mechanical sensors or power electronic converters. The proposed approach is based on the Kuramoto oscillator model [2], where each generator is treated as a nonlinear oscillator within a consensus-driven interaction framework. Through cooperative coupling dynamics, the generators autonomously converge toward frequency synchronization with inherent fault tolerance.

The proposed architecture is implemented on an ESP32-S3 microcontroller, which performs real-time signal processing and control. Using analog conditioning of the three-phase voltages, a discrete SRF-dqPLL (Synchronous Reference Frame Phase-Locked Loop) algorithm estimates the instantaneous phase and frequency of each generator through Clarke and Park transformations. Synchronization is physically achieved via active load regulation using servo-rheostat actuators, allowing the generators to cooperatively accelerate or decelerate until reaching a synchronized operating condition.

Experimental results demonstrate bounded steady-state synchronization error despite measurement noise and actuator nonlinearities, validating the feasibility of implementing nonlinear consensus-based synchronization on resource-constrained embedded hardware. The proposed platform therefore constitutes a resilient proof-of-concept for consensus-based synchronization in micro-generation systems governed by distributed dynamics [3].

Compared with conventional synchronization methods, the Kuramoto-based strategy offers several advantages. Droop control introduces steady-state frequency deviations and typically requires accurate active and reactive power measurements [4], while hierarchical Master-Slave approaches depend on a reference leader whose failure may compromise system stability [5]. In contrast, the proposed methodology achieves zero relative steady-state frequency error while enabling dynamic network reconfiguration after node failures.

Previous studies on Kuramoto-based synchronization in power systems have mainly focused on analytical models, numerical simulations, and large-scale smart-grid dynamics [6], [7], [3]. More recent works have explored consensus-based synchronization in inverter-dominated microgrids and distributed energy systems [8], [9]. However, practical embedded implementations operating under real-time and computational constraints remain comparatively limited [10], [11]. In particular, the integration of real-time dqPLL estimation, mean-field Kuramoto consensus, hybrid load regulation, and dynamic fault reconfiguration within a low-cost embedded platform has received limited experimental validation.

The principal contribution of this work is the experimental validation of a low-cost embedded implementation of Kuramoto-based synchronization for PMSG micro-generators under real-time operating conditions. Unlike conventional analytical or simulation-oriented approaches, the proposed architecture integrates dqPLL estimation, mean-field consensus dynamics, hybrid multi-rate control, and dynamic fault reconfiguration within a resource-constrained ESP32-S3 platform.

Throughout this paper, standard mathematical notation is adopted. Subscript i denotes the i-th generator. $v_{abc,i}$ represent the stator voltages with synchronous frame projections v_d and v_q. The hat ($\hat{x}$) indicates estimated variables. $\hat{f}_i$ and $\bar{f}$ are the local and mean-field centroid frequencies (in Hz), respectively. Ψ is the global phase centroid, and M defines the cardinality of the active generator set $\mathcal{A}$. For actuation, the control signal u_i and its discrete increment Δu_i govern the servo-rheostat angular position $\alpha_i \in [0°, 180°]$.

II. METHODOLOGY

A. Electrical State Estimation (SRF-dqPLL)

For real-time distributed control, continuous local state estimation is required. Since PMSG electrical dynamics

*This work was supported by Secretaria de Ciencia, Humanidades, Tecnología e Innovación (SECIHTI) México

[1]All the Authors are with Department of Science and Technology, CULagos, University of Guadalajara. Av. Enrique Díaz de León No. 1144, Colonia Paseos de la Montaña, Lagos de Moreno,Zip Code: 47460, Jalisco, Mexico.
[†]corresponding author: juan.onofre@academicos.udg.mx

depend on angular velocity (ω_m) and phase angle (θ), the three-phase stator voltages (v_a, v_b, v_c) are projected onto a synchronous rotating reference frame (dq) via sequential Clarke and Park transformations [12].

Each generator i employs a classic SRF-dqPLL [13]. Assuming small deviations, a proportional-integral (PI) filter minimizes the quadrature error $v_q \approx V_m(\theta_i - \hat{\theta}_i)$. A digitally controlled oscillator (DCO) then integrates the estimated frequency $\hat{\omega}_i$ to extract the phase $\hat{\theta}_i$ [14]. To prevent integration windup during low-voltage states (generator at low speed or powered off), a conditional gate pauses the integrator. The discrete difference equations, operating at $f_s = 2$ kHz ($T_s = 500\mu s$), are defined as:

$$\hat{\omega}_i[k] = K_p v_q[k] + K_i \sum_{n=0}^{k} v_q[n] T_s \tag{1}$$

$$\hat{\theta}_i[k] = \mod\left(\hat{\theta}_i[k-1] + \hat{\omega}_i[k]T_s, 2\pi\right) \tag{2}$$

To mitigate electro-mechanical ripple, the instantaneous estimation $\hat{\omega}_i[k]$ is processed through a first-order low-pass filter to obtain the smoothed frequency $\hat{f}_i$:

$$\hat{f}_i[k] = \alpha \hat{f}_i[k-1] + (1-\alpha)\frac{|\hat{\omega}_i[k]|}{2\pi} \tag{3}$$

where $\alpha = 0.95$ is the smoothing coefficient and the result is expressed directly in Hertz.

B. Frequency Consensus via the Kuramoto Model

This work replaces classical hierarchical topologies with a distributed control scheme modeled via Kuramoto's coupled oscillators. The phase dynamics of node i in an N-generator network are governed by [15]:

$$\dot{\theta}_i = \omega_{nom,i} + \frac{K}{N}\sum_{j=1}^{N} A_{ij}\sin(\theta_j - \theta_i) \tag{4}$$

where $\omega_{nom,i}$ is the natural frequency of the oscillator, K is the global coupling gain, and A_{ij} represents the adjacency matrix defining the communication topology.

Synchronization requires convergence to a common rotational speed, such that $\lim_{t\to\infty} |\hat{\omega}_{f,i}(t) - \hat{\omega}_{f,j}(t)| = 0$. However, computing pairwise interactions (Equation 4) becomes computationally prohibitive on the microcontroller as the network scales.

To optimize execution, the system employs Mean-Field coupling [2]. Avoiding pairwise calculations, it extracts an instantaneous network centroid—comprising a mean frequency ($\bar{f}$) and global phase (Ψ)—derived from the oscillators vector average:

$$\bar{f}[k] = \frac{1}{M}\sum_{i\in\mathcal{A}} \hat{f}_i[k] \tag{5}$$

$$\Psi[k] = \text{atan2}\left(\sum_{i\in\mathcal{A}} \sin(\hat{\theta}_i[k]), \sum_{i\in\mathcal{A}} \cos(\hat{\theta}_i[k])\right) \tag{6}$$

where $\mathcal{A}$ is the set of $M \leq 3$ active generators. Consequently, the phase control error $e_{\theta,i}$ is defined strictly by its deviation from the mean field:

$$e_\theta[k] = \sin\left(\Psi[k] - \hat{\theta}_i[k]\right) \tag{7}$$

This non-linear error acts as an attractive force that drives the units to cooperatively accelerate or decelerate toward the centroid. An additional advantage of the adopted mean-field formulation is its reduced computational complexity compared to conventional pairwise Kuramoto coupling strategies. Since the controller computes a global synchronization centroid rather than evaluating all pairwise oscillator interactions, the computational burden grows approximately linearly with the number of active nodes. This characteristic makes the proposed approach more suitable for embedded implementations operating under constrained real-time resources. To ensure resilience, the system continuously monitors node states. If a generator's voltage drops below 0.5 V, its dqPLL freezes integration, outputting 0 Hz. Additionally, nodes operating below $f_{min} = 10$ Hz are designated inactive and removed from $\mathcal{A}$.

Consequently, $M \leq 3$ updates in the next cycle, recalculating the centroid exclusively with active nodes. Simultaneously, the inactive node's servo saturates (180°) to shed its resistive load, facilitating a physical restart without disrupting the surviving network's synchronization.

C. Multi-rate Control Law for Load Regulation

Physical frequency consensus is achieved by modulating the PMSG resistive loads via servomotors. Operating at $f_{ctrl} = 20$ Hz through a decimation factor $N_{dec} = 100$, the mechanical control law combines viscous damping, Kuramoto phase attraction, and integral action to overcome inertia and steady-state errors. This multi-rate execution optimizes microcontroller resources [16].

The frequency error $e_{f,i}[k] = \bar{f}[k] - \hat{f}_i[k]$ and the phase difference $e_{\theta,i}[k] = \Psi[k] - \hat{\theta}_i[k]$ (strictly normalized within the interval $[-\pi, \pi]$) govern the discrete control equation. For physical actuation, the algorithm calculates a control increment $\Delta u_i[k]$:

$$\begin{aligned}\Delta u_i[k] = &\underbrace{K_{DAMP} e_{f,i}[k]}_{\text{Viscous Friction}} + \underbrace{K_{KUR}\sin(e_{\theta,i}[k])}_{\text{Transient Coupling}} \\ &\underbrace{+ K_{I,f}\sum_{n=0}^{k} e_{f,i}[n]\Delta t}_{\text{Frequency Integration}} + \underbrace{\gamma_i[k] K_{I,\theta}\sum_{n=0}^{k} e_{\theta,i}[n]\Delta t}_{\text{Hybrid Phase Integration}}\end{aligned} \tag{8}$$

where $\Delta t = N_{dec} T_s$ is the update period of the mechanical loop.

In this formulation, the proportional friction term (K_{DAMP}) acts as the primary mechanism to minimize the velocity error relative to the mean field, while the frequency integrator ($K_{I,f}$) establishes the nominal operating point by overcoming mechanical inertia differences. Simultaneously, the non-linear Kuramoto term (K_{KUR}) injects a corrective force that compels the generators toward magnetic-like attraction.

From a control perspective, the proposed strategy combines dissipative frequency damping with nonlinear attractive coupling dynamics inspired by the Kuramoto synchronization framework. The damping and bounded integral actions contribute to reducing frequency mismatch and preventing excessive oscillatory behavior, while the hybrid activation logic limits integral accumulation during large transients. Although a formal nonlinear stability proof of the complete hybrid system is beyond the scope of this work, the adopted control structure is experimentally observed to exhibit robust convergence toward synchronized operating conditions under all tested scenarios.

To prevent transient instability, a hybrid activation function $\gamma_i[k]$ activates the phase integrator ($K_{I,\theta}$) exclusively near synchronization ($|e_{f,i}| < 1.0$ Hz, $|e_{\theta,i}| < 1.0$ rad). Outside this region ($\gamma_i = 0$), the accumulated integral decays exponentially via a leakage factor ($\lambda = 0.95$) rather than resetting abruptly, ensuring smooth control transitions without discontinuous jumps [17].

Finally, the control increment is subjected to a dynamic rate-of-change limiter (*Slew Rate*, S_{max}) to protect the servomotor gears from erratic movements, yielding a bounded increment:

$$\Delta u_{i,lim}[k] = \max\left(-S_{max}, \min(S_{max}, \Delta u_i[k])\right) \tag{9}$$

The final angular position of the servomotor $\alpha_i[k]$, coupled to the rheostat, is updated integratively ($\alpha_i[k] = \alpha_i[k-1] + \Delta u_{i,lim}[k]$), ensuring its saturation within the physical range $[0°, 180°]$ through anti-windup logic [17]. Thus, although the primary goal of the micro-generation network is frequency synchronization, the inclusion of this hybrid logic and the coupling terms further enables strict intermittent angular alignment in steady-state.

The complete signal flow of this distributed topology is presented in the diagram shown in Figure 1.

D. Embedded Architecture and Experimental Setup

The proposed micro-generation synchronization platform was experimentally validated using a testbench consisting of three PMSG subsystems driven by DC motors, which emulate wind turbine dynamics. Although the synchronization dynamics are formulated from a distributed consensus perspective based on the Kuramoto model, the experimental implementation was intentionally realized using a centralized embedded architecture for proof-of-concept validation. All estimation, consensus, and control routines were executed on a dual-core ESP32-S3 (Espressif Systems) operating at 240 MHz. The physical experimental setup, comprising the three generation and control subsystems, is shown in Figure 2. Instrumentation was implemented using Hall-effect voltage sensors (LV25-P). Since the ESP32 requires unipolar signals within the 0 to 3.3V range, analog stages using operational amplifiers were designed to scale the three-phase voltages and introduce a continuous DC offset, enabling symmetrical digitization via the internal 12-bit ADCs.

Because the consensus logic is executed within a single centralized microcontroller, the communication between the virtual nodes occurs instantaneously. Consequently, network latency, communication are absent in this experimental setup. The only operational latency corresponds to the algorithmic execution time, which is bounded by the $T_s = 500\mu s$ hardware interrupt window.

Assuming a fully connected topology ($N = 3$), the algorithm continuously monitors unit status. The centroid Ψ averages the spatial vectors of active generators exceeding the voltage threshold. Failing or decelerating units are instantly isolated by the ESP32, updating the consensus ($N = 2$) to ensure uninterrupted Kuramoto operation for the remaining nodes. Table I details the system parameters.

TABLE I: Control Parameters and System Specifications

Parameter	**Symbol**	**Value**
Control System (ESP32)		
Update Frequencies (PLL)	f_s	2.0 kHz
Sampling Time	T_s	500 μs
Decimation Factor (Mechanical Control)	N	100
Resolución ADC	R_{adc}	12-bit
dqPLL Sintonization		
Proportional Gain	$K_{p,pll}$	4.6
Integral Gain	$K_{i,pll}$	261.8
Load Control (Servo)		
Proportional Gain	$K_{p,load}$	4.0
Integral Gain	$K_{i,load}$	50.0
Servo Actuation Range	α	$[0°, 180°]$

Unlike conventional Kuramoto-based studies primarily focused on analytical or simulation frameworks, the proposed implementation addresses real-time execution constraints on resource-limited embedded hardware. The integration of dq-PLL estimation, mean-field consensus dynamics, multi-rate control scheduling, and dynamic node reconfiguration within a single low-cost ESP32-S3 platform constitutes the principal practical contribution of this work.

III. Results

Experimental validation demonstrates both synchronization performance and the feasibility of executing consensus-based nonlinear dynamics under strict real-time embedded constraints using low-cost hardware. This architecture was validated in three stages: (1) transient and steady-state evaluation of the dqPLL estimator, (2) computational overhead verification, and (3) dynamic response of the Kuramoto frequency consensus.

A. State Estimator Validation (SRF-dqPLL)

Accurate local estimation is vital for consensus. Figure 3 illustrates the SRF-dqPLL startup transient. Demonstrating robustness against noise and harmonics, the algorithm achieves rapid frequency locking to provide reliable inputs for the Kuramoto control law.

The synchronization interval observed ($t < 7.0$ s) is consistent with the mechanical startup inertia of the PMSG units. The stability of v_d at 8 V, coupled with the vanishing

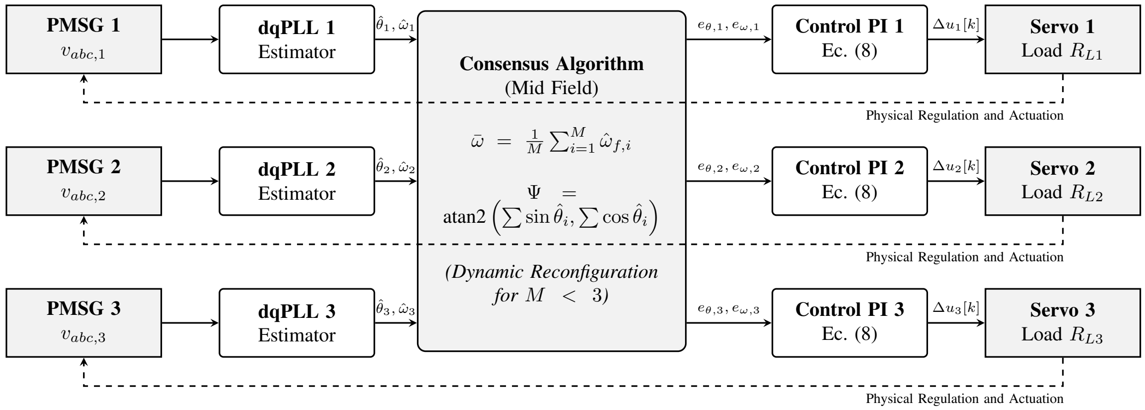

Fig. 1: Consensus-based synchronization architecture for three PMSG micro-generators implemented on a centralized embedded platform.

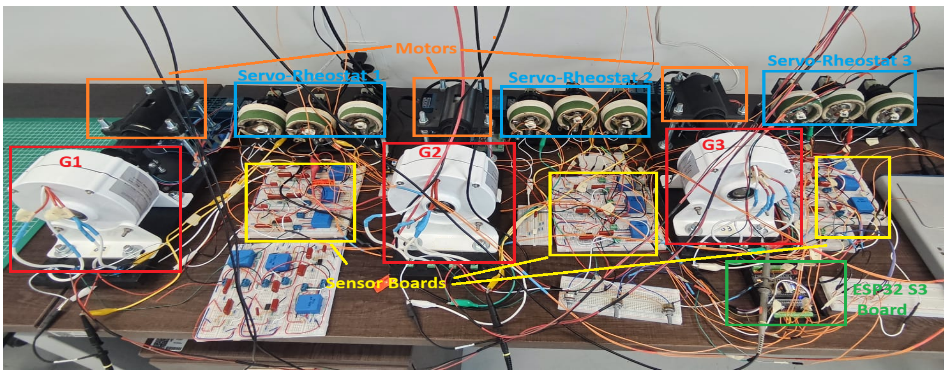

Fig. 2: Three PMSG coupled to their respective DC prime movers.

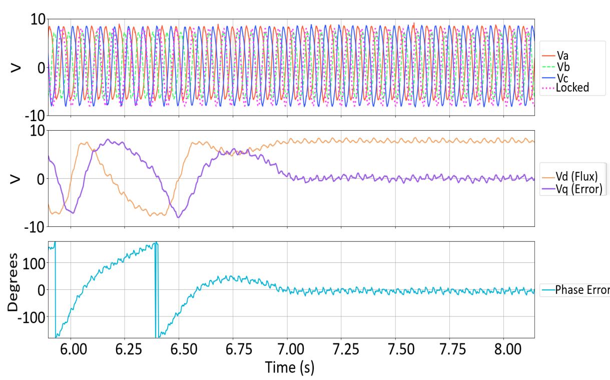

Fig. 3: Dynamic response of the SRF-dqPLL estimator: (Top) Three-phase voltages and locked phase signal. (Middle) Synchronous dq-frame components, demonstrating that $v_q \to 0$ at synchronization. (Bottom) Estimated phase angular error converging to steady-state equilibrium.

v_q component, validates the SRF-dqPLL's ability to extract clean state variables even under the non-linear acceleration profiles of the prime movers.

In steady-state ($t > 7.0$ s), the regenerated signal aligns with Phase-A, and the phase error converges to $0°$. A bounded ripple remains due to ADC noise and electro-mechanical harmonics, confirming the low-pass filter's ability to yield a stable phase reference.

B. Execution and Processing Capacity

The feasibility of implementing network algorithms on low-cost platforms depends critically on the processing capacity to resolve electrical estimations in real-time. In the proposed topology for $N = 3$, the central controller must sample nine analog channels (three voltages per generator) and execute three simultaneous instances of the SRF-dqPLL algorithm within a strict interrupt window of $T_s = 500$ μs. This multi-tasking requirement demands high-efficiency execution to avoid task overrun and ensure the deterministic behavior of the frequency consensus.

C. Dynamic Response and Frequency Consensus

To evaluate the network performance under the Kuramoto model, the transient response of the generators was analyzed across varying initial conditions and the dynamic entry of new nodes into the micro-grid. Figure 4 presents the temporal evolution of the estimated frequencies, the physical actuation of the servo-rheostats, and the relative error during the synchronization process.The results demonstrate that the Mean Field coupling effectively synchronizes the PMSG units even when starting from significant frequency offsets. The "plug-and-play" capability of the architecture is validated by the seamless integration of a third node ($N = 2 \to 3$), where the ESP32-S3 dynamically recalculates the consensus manifold without destabilizing the existing synchronized pair.

In the experimental scenario shown in Figure 4, the system

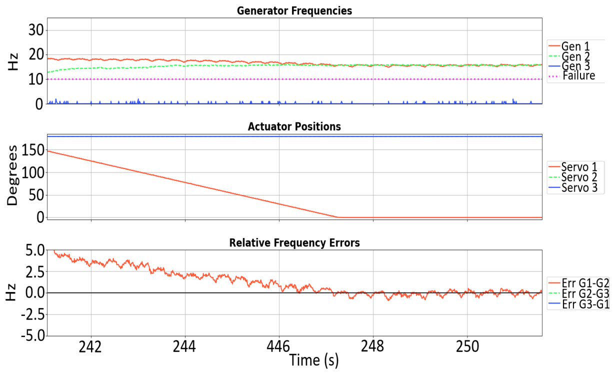

Fig. 4: Dynamic synchronization ($M = 2$). G_1 decelerates by increasing load (Servo 1 toward 0°) to match G_2. The inactive G_3 is excluded from the consensus, saturating its servo at 180° (null-load).

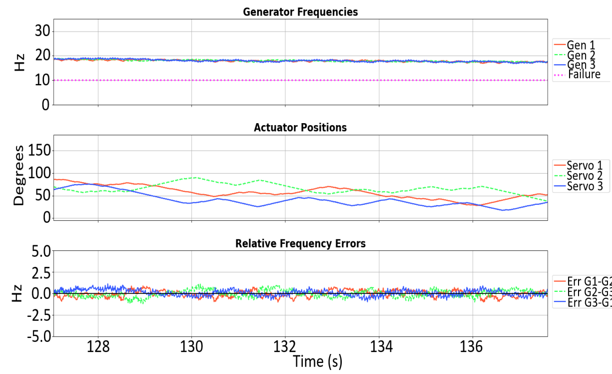

Fig. 5: Steady-state frequency consensus for $M = 3$. The three servomotors exhibit continuous dynamic actuation, evidencing the active rejection of mechanical perturbations and the compensation of inertia mismatches through the Kuramoto-based network.

begins with Generator 3 in an inactive state. The algorithm detects that $\hat{\omega}_{f,3} < f_{min}$ and promptly excludes it from the mean field calculation, dynamically operating the network with $M = 2$. Consequently, the control signal holds Servo 3 anchored at its saturation limit (180°), ensuring maximum resistance. This strategy effectively unloads the inactive node, minimizing electromagnetic torque and facilitating a potential future startup by reducing mechanical opposition.

Initially, Generator 1 operates at an approximate frequency of 18 Hz. Generator 2 is then integrated into the network at a lower frequency (≈ 13 Hz), inducing an initial relative error of 5 Hz between the two machines. Upon activating the coupling loop, the control law detects this deviation relative to the network centroid (Ψ). The ESP32-S3 then computes the necessary phase-velocity corrections, initiating a synchronized deceleration and acceleration process to bridge the frequency gap and achieve a stable consensus.

Cooperatively, G_1 decreases its servo position ($\approx 150° \to 0°$), lowering resistance to induce electromagnetic braking. Simultaneously, consensus forces slightly accelerate G_2, converging both to ≈ 16 Hz. The relative frequency error decays to 0 Hz, validating the decentralized mean-field synchronization.

Figure 5 demonstrates the steady-state performance of the distributed system operating at full capacity, with all three micro-generators active ($M = 3$). In this configuration, the network achieves a unified phase-lock, where the individual frequencies ω_i exhibit minimal deviation from the collective mean field Ψ. The synchronized operation with all three active generators demonstrates the capability of the proposed control law to maintain stable consensus under increased computational and control interaction demands within the validated experimental scale.

Finally, the empirical validation of the architecture concludes with a fault tolerance test. Figure 6 illustrates the system's behavior during the abrupt disconnection of one of the units ($M = 3 \to 2$). Upon the loss of a node, the mean field coupling instantaneously re-adjusts to the remaining active participants.As observed in the transient response, the frequency of the surviving cluster undergoes a momentary deviation before the Symmetric Multiprocessing (SMP) logic on the ESP32-S3 re-stabilizes the consensus manifold. This seamless transition without system-wide instability confirms the plug-and-play resilience of the decentralized Kuramoto law, ensuring that the micro-grid maintains operational continuity even under localized hardware failures.

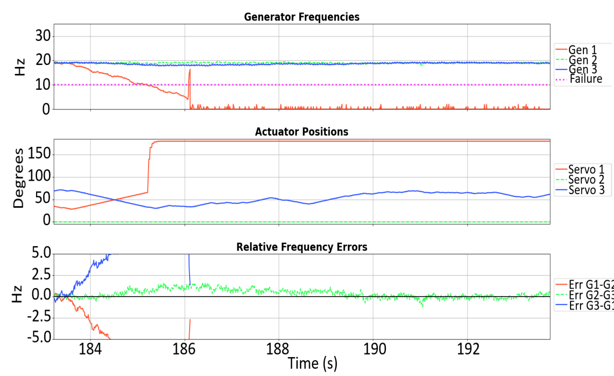

Fig. 6: System response to node failure. Dropping below 10 Hz, Generator 1 is excluded from consensus and its actuator saturated (180°). Generators 2 and 3 maintain stable phase-lock ($M = 2$), demonstrating decentralized resilience.

The experiment begins with the network operating in a steady-state global consensus ($M = 3$). At approximately $t = 183.5$ s, a total loss of mechanical torque occurs in the prime mover of Generator 1. The upper plot illustrates the subsequent decay of the estimated frequency $\hat{\omega}_{f,1}$. During this transient phase, the control loop attempts to compensate for the deceleration by increasing the position of Servo 1 toward 180° (minimum load), aiming to decrease the electrical resistance and unload the shaft to counteract the loss of kinetic energy.

The critical event occurs at $t \approx 185.5$ s, when the frequency of Generator 1 crosses the safety threshold ($f_{min} = 10$ Hz). The microcontroller detects the fault and executes the reconfiguration routine: it mathematically isolates the defective node, updates the mean field calculation to $M = 2$, and issues a forced saturation command to Servo 1. This causes an instantaneous jump to 180°, guaranteeing a null-load condition. This decisive action prevents the collapsing unit from draining energy from the active micro-grid, allowing the remaining nodes to stabilize their phase-lock without interference.

The success of the distributed topology is confirmed by observing the behavior of the remaining operational units (Generators 2 and 3). Despite the drastic perturbation introduced by the failure of Generator 1, the surviving nodes remain stable. The lower plot ratifies that the relative frequency error between G_2 and G_3 remains centered around zero both during and after the fault event. This seamless transition validates the resilience of the implemented Kuramoto-based network, demonstrating that the system is capable of isolating local faults and ensuring the operational continuity of the generation micro-grid.

D. Quantitative performance metrics

Table II summarizes key performance metrics. The dqPLL provides robust tracking (phase error $\leq \pm 5^\circ$, recovery 0.5–1.3 s). Physically, the Kuramoto consensus resolves a $\Delta f \approx 5\,\text{Hz}$ mismatch in ~ 7 s. Steady-state frequency errors remain bounded ($< \pm 1\,\text{Hz}$ balanced, $< \pm 1.75\,\text{Hz}$ disturbed), validating the multi-rate control's resilience against mechanical inertia and actuator limits.

TABLE II: Quantitative Performance Metrics of the Synchronization System

Performance Metric	**Measured Value**
Electrical Estimation (SRF-dqPLL)	
Phase Tracking Steady-State Error	$\pm 5^\circ$
Settling Time (Cold Start)	≈ 9.7 s
Settling Time (Dynamic Tracking)	$0.5 - 1.3$ s
Physical Consensus (Kuramoto Model)	
Convergence Time ($\Delta f \approx 5$ Hz step)	≈ 7.0 s
Steady-State Freq. Error (Balanced)	$< \pm 1$ Hz
Steady-State Freq. Error (Disturbances)	$< \pm 1.75$ Hz

IV. CONCLUSIONS

This work presented the design, implementation, and experimental validation of a low-cost embedded architecture for the synchronization of PMSG micro-generators. By employing a consensus scheme based on the Kuramoto oscillator model and utilizing a single ESP32-S3 microcontroller, the economic viability for micro-generation applications was successfully validated.

Experimental results confirmed that the coupling strength effectively drives independent generators to converge cooperatively toward a common frequency, successfully damping individual mechanical perturbations in steady-state. The most significant finding is the empirical verification of the network's robustness: the implemented system can detect a node's velocity loss, isolate it from the consensus manifold, and shed its resistive load without destabilizing the synchronism of the remaining operational units.

Consequently, the proposed architecture stands as a reliable and modular proof-of-concept platform for consensus-based synchronization in embedded micro-generation systems. Although the present validation was conducted using a three-node configuration, the obtained results suggest the feasibility of extending the proposed methodology toward larger multi-generator networks in future work. Nevertheless, larger-scale implementations will require further evaluation regarding communication overhead, timing determinism, and distributed execution constraints. Also, future work will address the formal nonlinear stability analysis of the proposed hybrid synchronization architecture, including convergence conditions under larger multi-generator configurations.

REFERENCES

[1] O. Ajala, A. D. Dominguez-García, and D. Liberzon, "An approach to robust synchronization of electric power generators," in *2018 IEEE Conference on Decision and Control (CDC)*, pp. 1586–1591, IEEE, 2018.

[2] J. A. Acebrón, L. L. Bonilla, C. J. Pérez Vicente, F. Ritort, and R. Spigler, "The kuramoto model: A simple paradigm for synchronization phenomena," *Reviews of modern physics*, vol. 77, no. 1, pp. 137–185, 2005.

[3] A. E. Motter, S. A. Myers, M. Anghel, and T. Nishikawa, "Spontaneous synchrony in power-grid networks," *Nature Physics*, vol. 9, no. 3, pp. 191–197, 2013.

[4] U. B. Tayab, M. A. B. Roslan, L. J. Hwai, and M. Kashif, "A review of droop control techniques for microgrid," *Renewable and Sustainable Energy Reviews*, vol. 76, pp. 717–727, 2017.

[5] A. Rincón-Silva, R. Rivera-Durón, and O. Orozco-López, "A low-cost embedded architecture for sensorless synchronization of pmsg-based micro-generators using load control," *Integration*, vol. 109, p. 102730, 2026.

[6] F. Dörfler and F. Bullo, "Synchronization in complex oscillator networks and smart grids," *Proceedings of the National Academy of Sciences*, vol. 110, no. 6, pp. 2005–2010, 2013.

[7] G. Filatrella, A. H. Nielsen, and N. F. Pedersen, "Analysis of a power grid using a kuramoto-like model," *The European Physical Journal B*, vol. 61, no. 4, pp. 485–491, 2008.

[8] A. Bidram and A. Davoudi, "Hierarchical structure of microgrids control system," *IEEE Transactions on Smart Grid*, vol. 3, no. 4, pp. 1963–1976, 2012.

[9] J. W. Simpson-Porco, F. Dörfler, and F. Bullo, "Synchronization and power sharing for droop-controlled inverters in islanded microgrids," *Automatica*, vol. 49, no. 9, pp. 2603–2611, 2013.

[10] D. E. Olivares, A. Mehrizi-Sani, A. H. Etemadi, *et al.*, "Trends in microgrid control," *IEEE Transactions on Smart Grid*, vol. 5, no. 4, pp. 1905–1919, 2014.

[11] J. M. Guerrero, J. C. Vasquez, J. Matas, L. G. de Vicuña, and M. Castilla, "Hierarchical control of droop-controlled ac and dc microgrids," *IEEE Transactions on Industrial Electronics*, vol. 58, no. 1, pp. 158–172, 2011.

[12] J. Aller Castro, *Máquinas Eléctricas Rotativas: Introducción a la Teoría General*. Sartenejas, Venezuela: Universidad Simón Bolívar, 2006.

[13] S.-K. Chung, "A phase tracking system for three phase utility interface inverters," *IEEE Transactions on Power electronics*, vol. 15, no. 3, pp. 431–438, 2000.

[14] Z. Ali, N. Christofides, L. Hadjidemetriou, E. Kyriakides, Y. Yang, and F. Blaabjerg, "Three-phase phase-locked loop synchronization algorithms for grid-connected renewable energy systems: A review," *Renewable and Sustainable Energy Reviews*, vol. 90, pp. 434–452, 2018.

[15] F. Dörfler and F. Bullo, "Synchronization in complex networks of phase oscillators: A survey," *Automatica*, vol. 50, no. 6, pp. 1539–1564, 2014.

[16] J. Ding, F. Marcassa, S.-C. Wu, and M. Tomizuka, "Multirate control for computation saving," *IEEE transactions on control systems technology*, vol. 14, no. 1, pp. 165–169, 2006.

[17] K. J. Astrom and T. Hägglund, "Advanced pid control," *IEEE Control Systems*, vol. 26, no. 1, pp. 98–101, 2006.